Enhanced NO2 gas sensing performance of Gd/Li co-doped ZnO thin films

Article *in* Indian Journal of Physics · May 2023

DOI: 10.1007/s12648-023-02761-5

Indian J Phys
https://doi.org/10.1007/s12648-023-02761-5

ORIGINAL PAPER

Enhanced NO_2 gas sensing performance of Gd/Li co-doped ZnO thin films

K K Jasmi[1]*, T A Johny[1], V S Siril[2] and K N Madhusoodanan[2]

[1]Department of Physics, St. Thomas' College, Affiliated to University of Calicut, Thrissur 680001, India

[2]Department of Instrumentation, Cochin University of Science and Technology, Cochin 682022, India

Received: 26 October 2022 / Accepted: 25 April 2023

Abstract: In this paper, we demonstrate pure, Gd-doped, and Gd/Li co-doped ZnO nanostructures for NO_2 gas sensing applications fabricated via the sol–gel spin coating route. The synthesized samples are examined through various characterization techniques to evaluate their physical and chemical properties. The gas sensing performance of all deposited samples was investigated at different temperatures (150–240 °C) towards 75 ppm of NO_2 gas. Among them, the Gd/Li co-doped ZnO sample shows remarkable NO_2 gas sensing performance of 55.18 at a working temperature of 210 °C. Also, the gas sensitivity of Gd/Li: ZnO towards various toxic gases, including Cl_2, NH_3, NO, and NO_2, were studied and appeared most selective towards NO_2 gas. A possible NO_2 gas sensing mechanism was discussed and correlated with structural, morphological, electrical, and spectral studies.

Keywords: Gd/Li co-doped ZnO; NO_2 gas sensor; Selectivity; Stability; Sensitivity

1. Introduction

A huge variety of hazardous gases are emitted into the atmosphere due to industrialization and urbanization, including H_2S, CO_2, NH_3, NO_2, Cl_2, etc., which causes many health issues. So, gas sensors with low optimum temperatures, remarkable sensitivity, strong stability, and outstanding repeatability are essential for monitoring these gases. Nitrogen dioxide (NO_2), a major air pollutant among them, is produced by the burning of fossil fuels, which leads to acid rain and respiratory ailments. So it is critical to monitor NO_2 gas levels quickly and precisely to maintain their value below the exposure limit [1]. Among the gas sensors, chemiresistive gas sensors, are considered promising materials with simple working principles, cost-effectiveness, stability, and efficient with a low working temperature[2].

ZnO is widely employed in various applications, including light-emitting diodes, photocatalytic activity, gas sensors, solar energy conversion, storage devices, and more, owing to its desirable features, including a large band gap, high exciton binding energy, low cost, nontoxicity, and broad availability [3–7]. Although ZnO is a promising material for gas sensor devices, it has numerous drawbacks, such as high optimum temperature, limited gas sensitivity, and low reliability, which may restrict its gas sensing applications. The literature review reveals that adding dopants or co-dopants improves the gas sensitivity of the host material by changing the surface morphology of the host material. As a result, the surface-to-volume ratio increases, and defects are formed, which may facilitate the gas sensing capabilities of ZnO.

However, dopant addition is the simple and effective technique to enhance the gas-sensing capabilities of ZnO. Many works have been carried out to develop various topologies to circumvent these restrictions, including porous, nanocomposite, and hetero-structured ZnO [8–11]. Several metal elements, including transition metals, rare earth materials, alkali metals, etc., were doped into ZnO to increase NO_2 gas sensing capabilities [12–16]. Instead, alkali metal (Li) and rare earth element (Gd)-doped ZnO demonstrates enhanced gas sensitivity because of its catalytic nature, high surface-to-volume ratio, and rapid mobility of oxygen ions, which will improve the free electron conductivity [17–19]. As a result, a large number of active sites are formed for gas adsorption on the surfaces of the sample. Since, the Gd^{3+} (93 pm) has a larger ionic

*Corresponding author, E-mail: jasmifirdhouse@gmail.com

Published online: 18 May 2023

radius than that of the Zn^{2+} (74 pm), intrinsic defects are formed such as Zn-interstitial and vacancy, as well as O-interstitial and vacancy, that enhance the gas sensing capabilities. Besides, when compared to other rare earth ions, Gd^{3+} possesses energy levels that are in the conduction band of ZnO, which improves the possibility of a significant modification in the energy distribution of the host ZnO [18]. Additionally, Li^{+} (60 pm) has a shorter ionic radius than Zn^{2+}, making it easy to enter the ZnO matrix and provide a selective, sensitive gas sensor with quick response and recovery durations. Therefore, for improved gas sensing applications, numerous groups have concentrated on alkali metals or rare earth elements. Only a few groups focused on co-dopant to enhance gas sensing properties including Co-In, Fe-In, Al-Sn, Al-Ga, N-F, Al–Mg, Mn-Ni, doped ZnO, etc. [10, 19–24].

In this scenario, pure, Gd:ZnO, and Gd/Li co-doped ZnO nanostructures were fabricated via a facile and inexpensive sol–gel spin coating route. The synthesized samples were characterized through XRD, FESEM, a four-probe Hall measuring system, photoluminescence (PL), and UV–Visible spectroscopy. Furthermore, various gas sensing parameters, such as temperature dependence dynamic response, stability, selectivity, repeatability, and response/recovery duration towards various concentrations of NO_2 gas were measured. The gas sensing mechanism of the deposited samples were discussed and correlates with the structural, spectral, morphological, and electrical parameters of the deposited samples. The Gd/Li:ZnO sensor is established as a promising material in the present work for the detection of harmful NO_2 gas present in the atmosphere.

2. Experimental details

2.1. Film deposition technique

Required solutions (0.5 M) of undoped ZnO, 0.5 wt.% Gd-doped ZnO, and 0.5 wt.% Gd and 1 wt.% Li co-doped ZnO were prepared by mixing zinc acetate dihydrate, gadolinium acetate tetrahydrate, and lithium acetate dihydrate with diethanolamine as a stabilizer and isopropyl alcohol as a solvent. stirred the mixture at room temperature till the solution became transparent and kept it for 48 h for stability. All the chemicals used are ACS-grade, which can be used without any further purification. Before deposition of the film onto the glass substrate, the substrate is cleaned using acetone followed by an ultrasonic cleaner to ensure film clarity. Deposit the precursor solution using a spin coater, then keep it in an oven followed by a furnace at 150 °C for 20 min and 500 °C for 30 min, respectively [25].

2.2. Film characterization tools

The crystal structure properties were collected from an X-ray diffractometer (XRD, Pan Analytical) with a wavelength of 154 pm and surface morphology was measured by FE-SEM, Carl Zeiss Supra, 40VP, elemental composition and defect states were obtained from XPS (Axis Ultra), UV–visible and photoluminescence spectra were measured from JASCO, V-780. Electrical parameters were investigated with a four-probe Hall measurement system (HMS-3000, Ecopia, S. Korea) used to study the electrical conductivity of the prepared sensors. The samples were in ohmic contact with the apparatus using silver paste. The gas sensing parameters of pure, Gd:ZnO and Gd/Li:ZnO thin-film sensors were measured using Keysight (34461A, 6.5 resolution) multimeter while exposed to various concentrations of NO_2 gas at an optimal temperature of 210 °C. The electrical connections from the sensor are made with the help of two thin copper wires connected to the thin film with silver paste. The gas sensing setup was preheated at 500 °C to ensure a moisture-free environment for gas sensing measurement [26].

3. Results and discussion

3.1. Structural study

The XRD spectra of deposited thin film samples as illustrated in Fig. 1(a). All patterns indicate hexagonal wurtzite structure according to JCPDS card no. 01-0709-0205 [15]. The diffraction peak of Gd:ZnO and Gd/Li:ZnO shows slight shift towards lower side of diffraction angle compare to pure ZnO, which indicates dopant or co-dopants substitute interstitially into ZnO matrix [27]. There are no extra peaks linked with the dopant and co-dopant, indicating a low concentration of dopant. Here, the co-dopants, Gd^{3+} (93 pm) and Li^{+} (60 pm), readily reach the interstitial site without disrupting the structure with an increase in FWHM. Crystallinity decreases as the FWHM of diffraction peaks increases. For more clarity, the crystallite size of the (002) peak was determined using Scherrer's equation: $D = Kl/bcosq$, k defined Scherrer's constant (= 0.9), l is the wavelength of the Cu-K α radiation, q is the Bragg's angle and b is FWHM (full-width half maximum) as shown in Table 1. The reduction in crystallite size is due

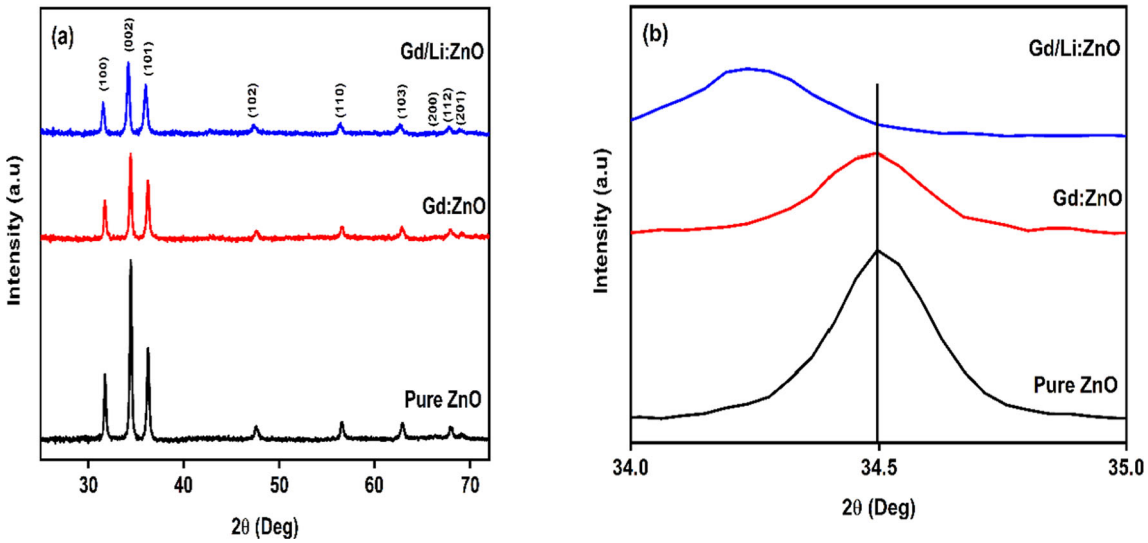

Fig. 1 (**a**) XRD spectrum, and (**b**) Zoomed pattern of (101) peak of deposited thin films

Table 1 XRD parameters of the deposited samples

Thin film	Lattice constants (Å)		FWHM (β)(deg)	Crystallite size (nm)	Strain (10^{-3})
	a = b	c			
Pure	3	5.2	0.2587	30.73	1.1282
Gd:ZnO	3	5.2	0.2636	30.16	1.1495
Gd/Li:ZnO	3.02	5.23	0.3288	24.16	1.4350

to more oxygen vacancies are formed after doping Gd and Gd/Li [28]. Also, the strain of the crystal system was estimated using the equation, $\mathcal{E} = bcosq/4$.

3.2. FE-SEM analysis

FE-SEM analysis was used to obtain the apparent morphologies and particle distribution histograms of the deposited samples, as shown in Fig. 2(a)-(c). In pure ZnO nanoparticle formation exhibits both a spherical and an irregular morphology with aggregated particles. For Gd:ZnO and Gd/Li:ZnO demonstrates a tendency to grow morphologies that resemble nanorods with a porous structure that serves as an active site for the test gas, compared to pure ZnO. According to the histogram of particle distribution, the average grain sizes for pure ZnO, Gd:ZnO, and Gd/Li:ZnO were found to be 20.29 nm, 17.46 nm, and 13.13 nm, respectively, which shows good agreement with XRD data on crystallite size.

3.3. Electrical studies

The intrinsic n-type nature of the ZnO semiconductor is confirmed by hall measurements, Table 2(a). In Gd:ZnO, since Gd^{3+} (93 pm) has larger ionic radius than that of Zn^{2+} (74 pm), it may readily assimilate into the interstitial site without disrupting the geometry, resulting in n-type conductivity with higher carrier density, Table 2(b). Even though Li^{+} (60 pm) ions have a smaller ionic radius than Zn^{2+}(74 pm) ions, Li enters the lattice or interstitial site in Gd/Li:ZnO. As indicated in Table 2(c), Li enters the interstitial site with an increase in carrier density and a decrease in resistivity, shows good agreement with structural studies.

3.4. Optical studies

Gaussian multiple peak fit was used to analyse the photoluminescence spectra of pure, Gd:ZnO and Gd/Li:ZnO samples (Fig. 3). It verified the defect density states of the samples that had been developed. In the pure thin film sample, a peak is observed in the range of 366–390 nm, showing UV-emission, which is attributed to near band emission. The peak intensity of UV emission as well as a shift to a higher wavelength range 368.7–398 nm can be seen in ZnO:Gd and Gd/Li:ZnO. It's because Gd doping as well as Gd/Li co-doping narrowed the bandgap and caused non-luminescent recombination sites or defects. In the

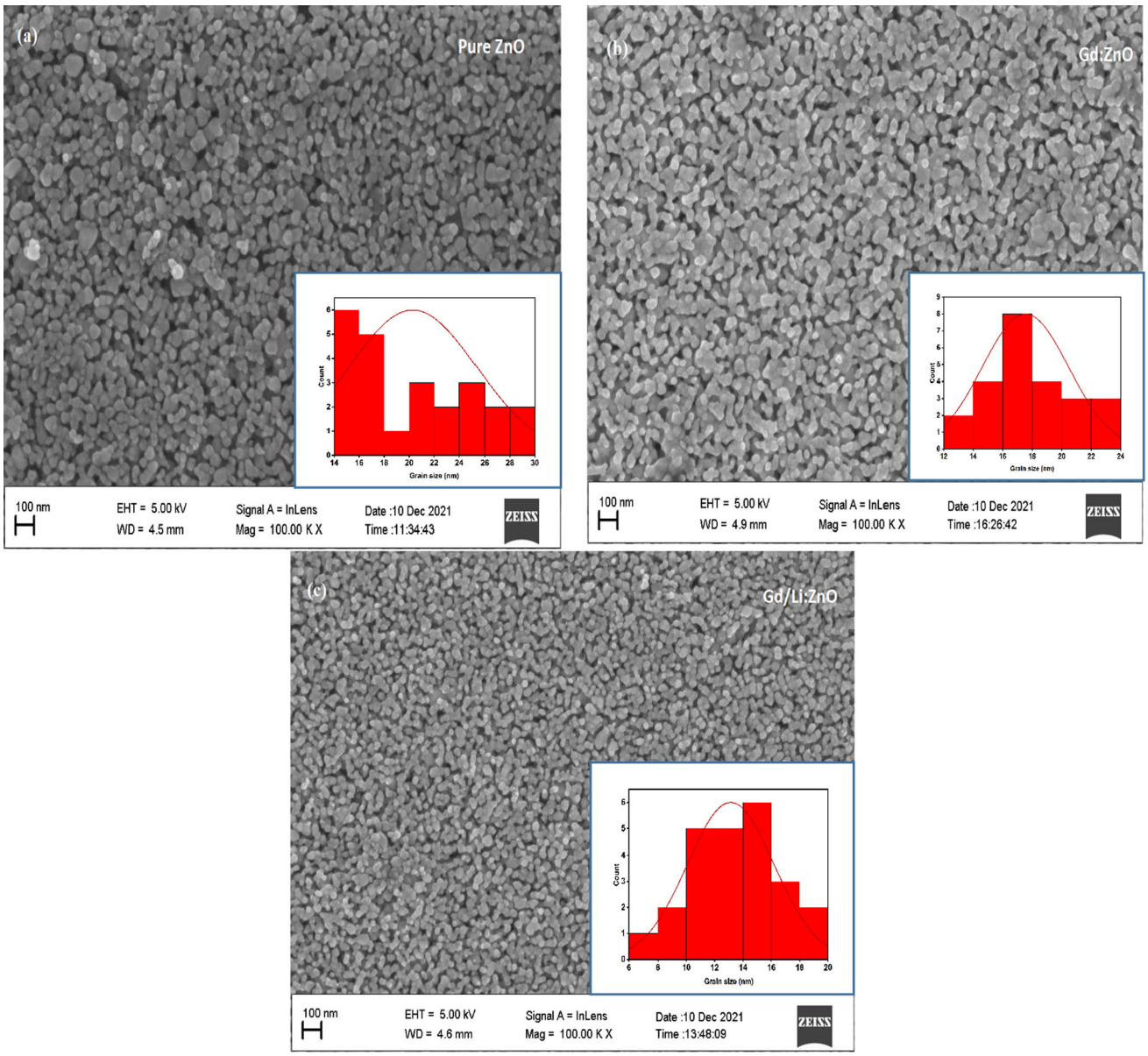

Fig. 2 (**a–c**) FE-SEM image and histogram of grain size distribution of deposited samples

Table 2 Four-probe hall measurement and gas sensing parameters of deposited thin films

Sl. No	Thin film	Resistivity (Ω cm)	Carrier-density (per cm^3)	Type	Sensitivity	Response/recovery time (sec)
(a)	Pure ZnO	4.78×10^3	4.04×10^{15}	*n*	8.02	97/105
(b)	Gd:ZnO	2.81×10^2	2.81×10^{16}	*n*	17.25	62/86
(c)	Gd/Li:ZnO	2.57×10^1	5.82×10^{18}	*n*	55.18	15/27

visible range, violet, blue, and green correspond to wavelengths of 404–421 nm, 450–468 nm, and 507–546 nm, respectively. Imperfections at grain boundaries, such as interface traps, generate the violet band [17, 18]. Transitions between shallow acceptor levels (V_{zn}) shallow donor levels (Zn_i) and induce blue band emissions [29], whereas oxygen vacancies (donor defect) cause green band emissions [30]. The presence of vacancies and defects enhances the gas sensing applications of the deposited samples [31].

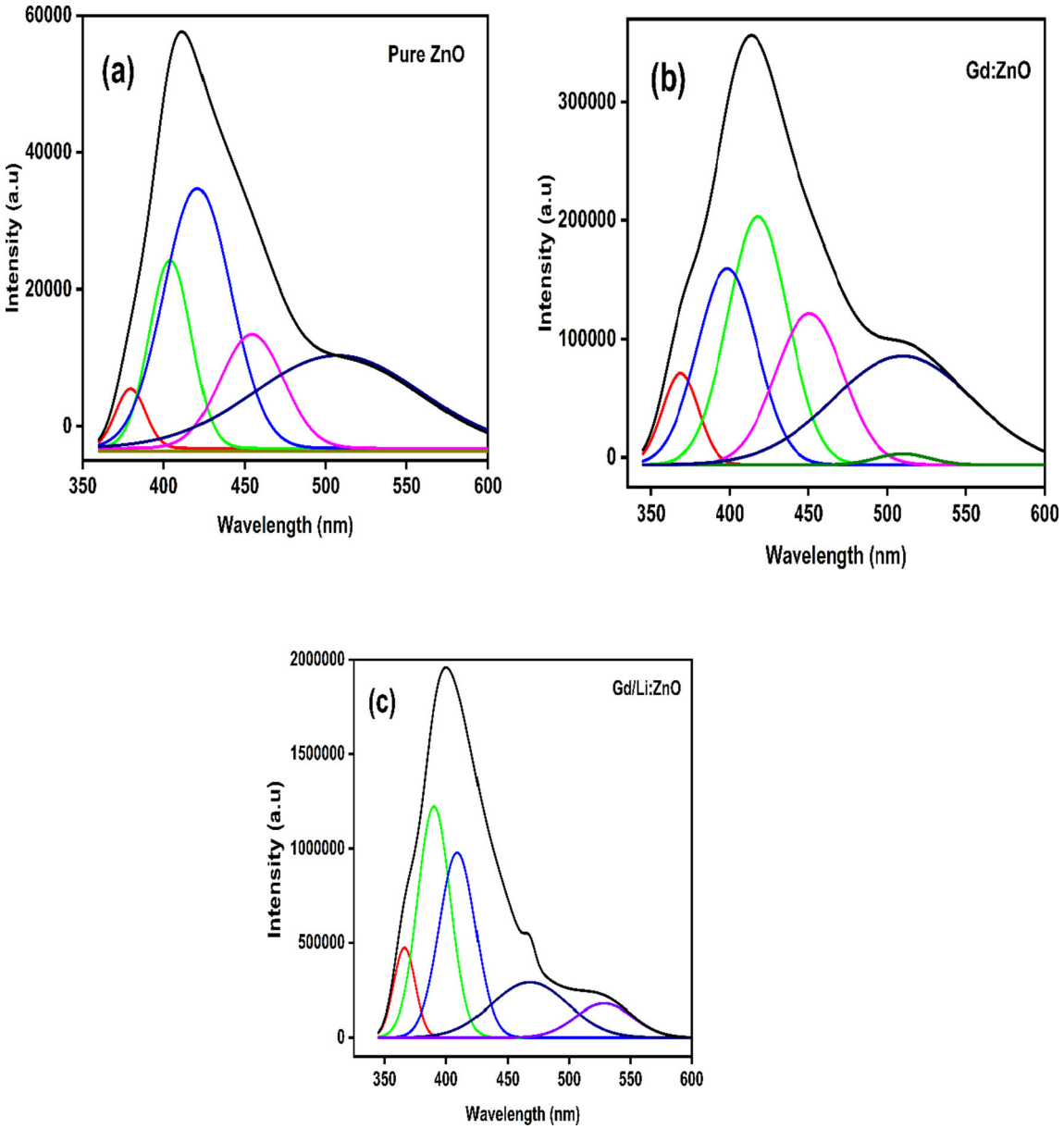

Fig. 3 (**a–c**) PL spectra of deposited thin films

The spectral characteristics of deposited samples were explored by UV–Vis transmission spectroscopy to study the impact of oxygen vacancies on the band gap energy of Gd/Li:ZnO, Fig. 4(a). The optical band gap of the nanostructure was measured using a Tauc plot, as shown in Fig. 4(b). Pure ZnO, Gd:ZnO, and Gd/Li:ZnO have band gap energies of 3.22 eV, 3.19 eV, and 3.17 eV, respectively. These findings clearly reveal that following the doping process, the band gap shrank due to oxygen vacancies [32]. The increase of oxygen vacancy enhances the gas sensitivity significantly [33].

3.5. XPS analysis

XPS was used to investigate at the prolonged influence of defect states in Gd/Li:ZnO thin film. We attempted to correlate the interstitial substitution of Gd^{3+} and Li^{+} ions in the presence of oxygen vacancy defects. No impurities were discovered while measuring the Gd/Li:ZnO XPS survey spectrum (Fig. 5a). To assess the impact of Gd and Li doping on a ZnO sample, high-resolution XPS spectra of Zn, Gd, Li, and O were collected. According to Fig. 5b, Zn 2p (Zn 2p3/2 and 2p1/2) has a binding energy of 1020.95 eV and 1044.05 eV, respectively. Using Gaussian

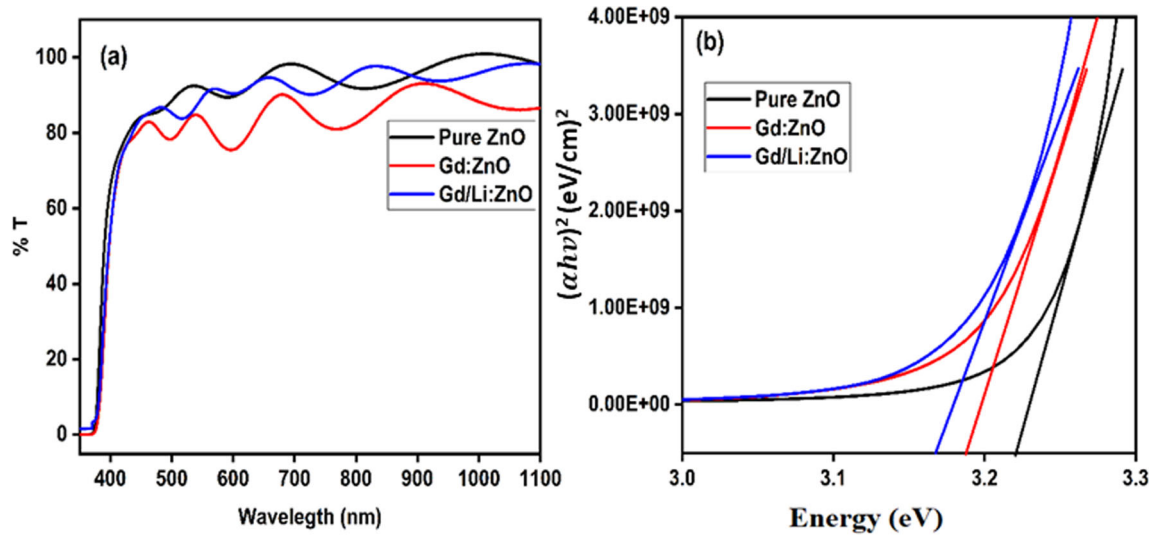

Fig. 4 (**a**) Transmission spectra and (**b**) $(\alpha hv)^2$ vs (hv) plot of the deposited thin films

multiple peak fit, the O 1 s peak can be split into low and high binding energy regions for Gd/Li:ZnO, which can be used to determine the oxygen vacancy (Fig. 5c). The low binding energy region is caused by the O^{2-} ions on the wurtzite structure of the hexagonal Zn^{2+} ion array, the high binding energy region is a result of the O^{2-} ions in oxygen-deficient zones and chemisorbed or dissociated oxygen or OH^- ion on the surface of ZnO nanocrystals. Additionally, the Gd-3d spectrum (Fig. 5d) confirms the presence of the Gd^{3+} state[34]. A lower binding energy curve that peaked at 52.25 eV is identified as lithium interstitial substitution (Li_i) defects from the XPS Li 1 s spectra (Fig. 5e), showing the n-type electrical conductivity, which is in good accordance with structural analysis.

3.6. Gas sensing studies

The gas sensitivity of metal oxide semiconducting gas sensors largely depends on their working temperature. Figure 6(a) illustrates, sensitivity-temperature dependence of all deposited thin film sensors operated at various temperatures from 150 to 240 °C. These films were found to be highly sensitive and showed a rapid response and recovery time towards NO_2 gas at all the selected temperature ranges. The response of the sensors was found to increase with operating temperature and peaked at 210^OC, which was considered as an optimum temperature. Low temperatures prohibit NO_2 gas from having enough energy to overcome the adsorption barrier. Furthermore, because the rate of desorption is larger than the rate of adsorption at high temperatures, sensitivity is reduced. The sensor's show maximum response occurs when the adsorption and desorption rates are equivalent at the optimum temperature.

The dynamic response of all deposited samples as a function of NO_2 gas concentration (15–75 ppm) is shown in Fig. 6(b). As NO_2 gas concentrations increase, the gas sensing response also increases. Here, Gd/Li:ZnO shows enhanced gas sensitivity and short response/recovery time compared to other deposited thin films. The selectivity studies carried out among toxic gases such as Cl_2, NH_3, NO and NO_2 (210^OC, 75 ppm), as shown in Fig. 6(c), the Gd/Li:ZnO thin film sensor showed a significant sensitivity towards NO_2 gas. Another important factor to consider is its stability, the response of this sensor was evaluated for 3 months to test its stability for the undoped and Gd/Li:ZnO sensor, as shown in Fig. 6(d). Compared to undoped ZnO, Gd/Li:ZnO shows good stability for a long time. The sensor's cyclic functioning is also a crucial aspect for device applications. The repeatability of Gd/Li:ZnO towards 75 ppm of NO_2 gas is shown in Fig. 6(e), and it exhibits good reproducibility.

4. Gas sensing mechanism

Chemiresistive sensors exploit changes in resistance after exposure to gas as the basis for their gas sensing mechanism [35]. The non-stoichiometric crystal defect in ZnO increases the surface area of free electrons and enhances the electrical resistance. The structural, electrical, and morphological characteristics are influenced by the dopant addition. This will promote the formation of interstitial and oxygen-vacancy defects. The adsorption of oxygen from

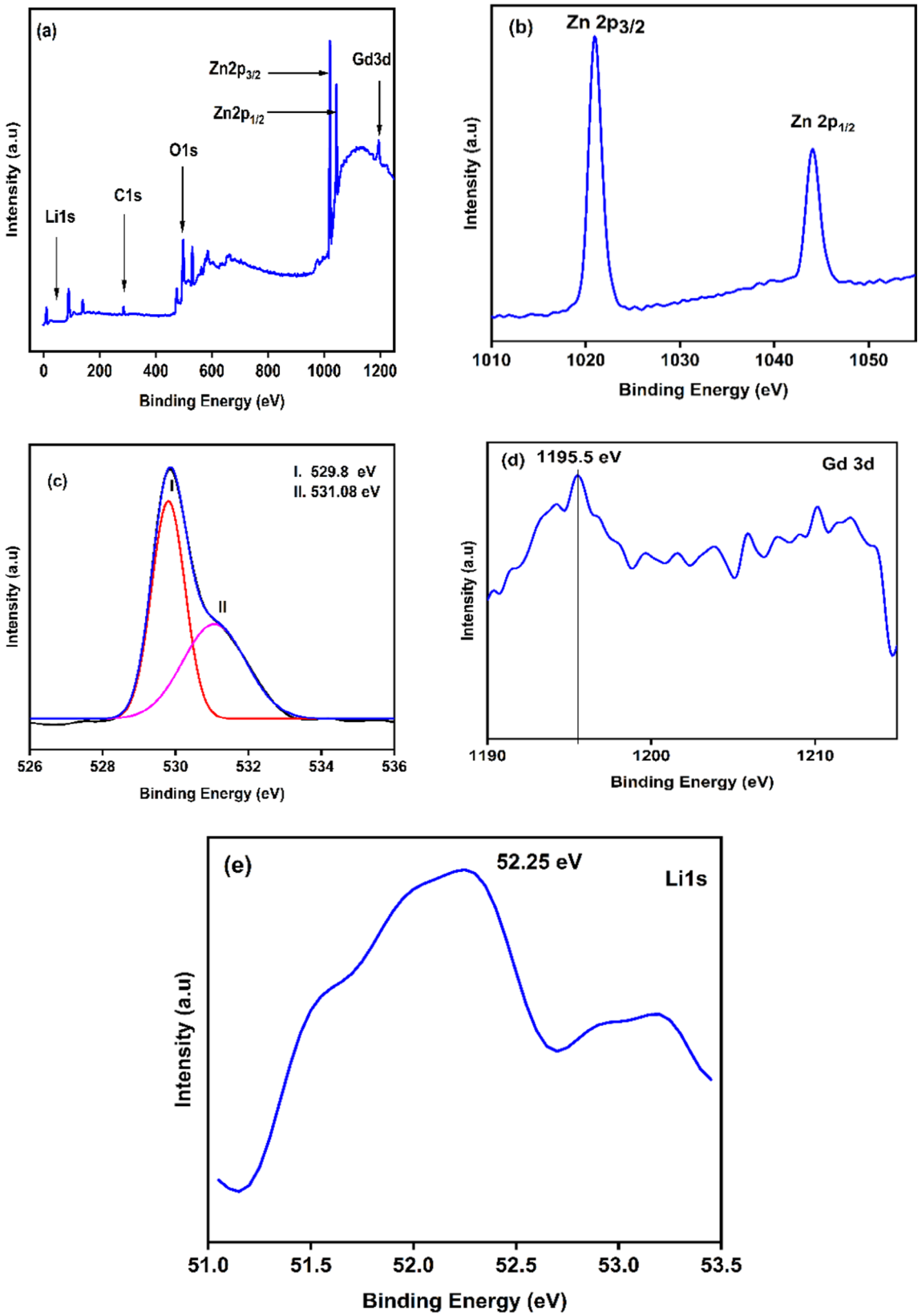

Fig. 5 (**a**) Survey, (**b**) Zn2p, (**c**) O1s, (**d**) Gd 3d, and (**e**) Li1s, XPS spectrum of Gd/Li:ZnO

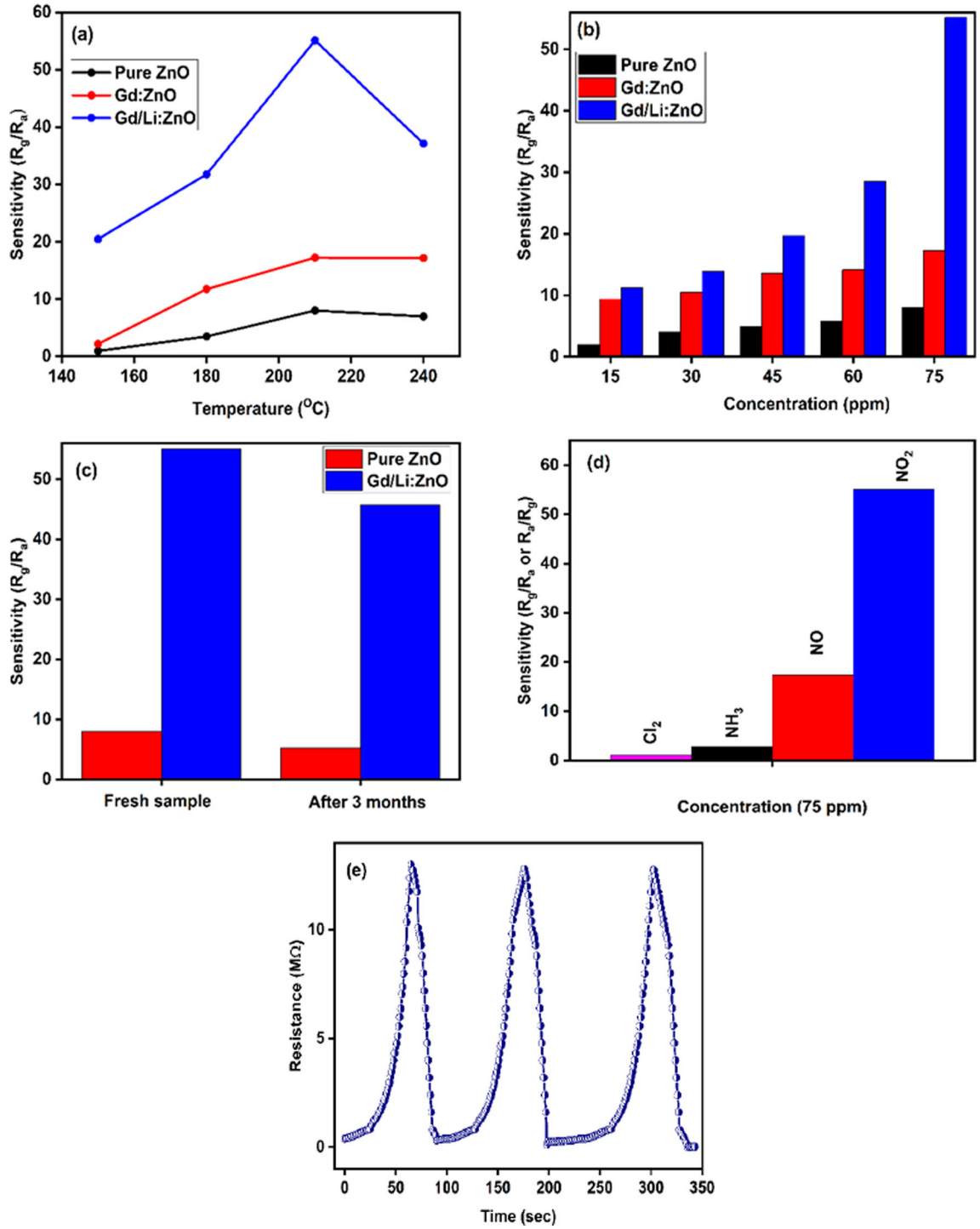

Fig. 6 (**a**) Temperature dependence plot of Gd/Li:ZnO, (**b**) Sensitivity- Concentration graph of deposited samples, (**c**) stability measure of pure and Gd/Li:ZnO thin films, (**d**) selectivity histogram of Gd/Li:ZnO, and (**e**) cyclic response of Gd/Li:ZnO

the air on the surface of ZnO has an impact on its electrical resistance. At ambient temperature, the O_2 molecules adsorbed on the surface of the ZnO thin film withdrawn electrons from the conduction band, resulting the formation of O_2^- as illustrated below [36, 37].

$$O_{2(gas)} \rightleftharpoons O_{2(adsorbed)} \quad (1)$$

$$O_{2(adsorbed)} + e^- \Longleftrightarrow O^-_{2(adsorbed)} \quad (2)$$

When the temperature is around 210^{O}C, the O_2^-/O^-

interact with free electrons, as per the following Eqs. (3) and (4) [38, 39].

$$O^-_{2(adsorbed)} + e^- \Longleftrightarrow 2O^-_{(adsorbed)} \quad (3)$$

$$O^-_{(adsorbed)} + e^- \Longleftrightarrow O^{2-}_{(adsorbed)} \quad (4)$$

When NO_2 gas is introduced, it interacts with the adsorbed as shown in the equation below (5)[40].

$$NO_{2(adsorbed)} + O^{2-}_{(adsorbed)} + 2e^- \Longleftrightarrow NO^-_{2(adsorbed)} + 2O^-_{(adsorbed)} \quad (5)$$

As a result, a potential barrier is formed with a positive charge in the semiconductor and a negative charge on the adsorbed gases. In the presence of NO_2 gas, the height of the barriers enlarges due to the abstraction of extra electrons from the surface of ZnO, resulting in an increase in sensor resistance. Additionally, because the gas sensor is n-type, it induces oxygen vacancies that serve as favourable sites for the adsorption of NO_2 gases and oxygen, resulting in better gas sensitivity; this result is also supported by the narrowing nature of band gap while adding dopant or co-dopant. Among the fabricated samples, a Gd/Li:ZnO thin film gas sensor with a porous structure along with a narrow band gap and a sufficient number of electrons is a promising candidate for enhanced NO_2 gas sensing applications.

5. Conclusions

In summary, transparent pure, Gd:ZnO and Gd/Li:ZnO thin films were synthesized via the facile sol–gel spin-coating route. The XRD study confirms that all deposited samples were polycrystalline with a hcp structure. The morphological analysis revealed that thin films with a small size are suitable for manufacturing gas sensors, as the surface area to volume ratio is high. Spectral studies confirm the presence of oxygen vacancies in all deposited samples. The Hall measurement of all deposited thin film samples shows n-type conductivity, and the sample with a larger carrier concentration provides a sufficient number of electrons that create more active sites for NO_2 gas adsorption. Among all deposited samples, the Gd/Li:ZnO shows a remarkable NO_2 gas sensitivity of 55.18 at an ideal temperature of 210 °C toward 75 ppm of NO_2 gas along with good stability, excellent selectivity, and reusability towards NO_2 gas. This work presented Gd/Li:ZO as a promising candidate for stable, selective, and sensitive NO_2 gas sensing applications.

References

[1] H Salonen and T Salthammer *Environ. Int.* **130** 104887 (2019)
[2] X Wang, T Wang, G Si, Y Li, S Zhang and X Deng *Sensors Actuators B. Chem* **302** 127165 (2020)
[3] M Nouri and S Mohammadnejad *Surf. Interfaces.* **28** 101666 (2022)
[4] M C Hidalgol, D Hern and G Nú *Journal of Photochemistry Photobiology A Chemistry.* **404** 112866 (2021)
[5] S S Khudiar, U M Nayef, F A Mutlak and S K Abdulridha *Optik (Stuttg).* **249** 168300 (2022)
[6] M Aamir, T Adhikari, M Sher, N Revaprasadu, W Khalid and J Akhtar *New J. Chem.* **42** 14104 (2018)
[7] A A Ahmad, A M Alsaad, Q M Al and B M Ali *Polym. Bull.* **78** 1189 (2021)
[8] M Sik Choi et al. *Appl. Surf. Sci.* **568** 150910 (2021)
[9] R Vyas, S Sharma, P Gupta, A K Prasad, A K Tyagi and K Sachdev *Adv. Mater. Res.* **585** 235 (2012)
[10] G S Hikku, R K Sharma, R V William, P Thiruramanathan, G S Hikku, R K Sharma, R V William and P Thiruramanathan *Integr. Med. Res.* **11** 576 (2018)
[11] B Sharma, A Sharma, M Joshi and J Myung *Chemosensors.* **8** 3 67 (2020)
[12] K K Jasmi, T A Johny, V S Siril, and K N Madhusoodanan *Mater. Today Proc.* (2022)
[13] V S Kamble, R K Zemase, R H Gupta, B D Aghav, S A Shaikh and J M Pawara *Opt. Mater. Amst.* **131** 112706 (2022)
[14] V S Kamble, Y H Navale, V B Patil, N K Desai and S T Salunke *J. Mater. Sci. Mater. Electron.* **32** 2219 (2021)
[15] R S Ganesh, V L Patil, E Durgadevi, M Navaneethan and S Ponnusamy *Chem. Phys. Lett.* **734** 136725 (2019)
[16] P Bharathi et al. *Appl. Surf. Sci.* **499** 143857 (2020)
[17] K Kasirajan, L B Chandrasekar, S Maheswari, M Karunakaran and P S Sundaram *Opt Mater (Amst.)* **121** 111554 (2021)
[18] D Sahu, N R Panda and B S Acharya *Materials Research Express.* **4** 11 114001 (2017)
[19] M William, K E Rammutla, T E Mosuang and B W Mwakikunga *Sensors Actuators B Chem.* **247** 228 (2017)
[20] B Sahoo, K J Sankaran, R Sakthivel, S Kumar and D Behera *Superlattices Microstruct.* **146** 106666 (2020)
[21] H J Al-asedy, N Bidin, S A Al-khafaji and H Bakhtiar *Mater. Sci. Semicond. Process.* **77** 50 (2018)
[22] K Ayeb, N Moussa, M Faouzi, S Gianluca and G Neri *Mater. Sci. Eng. B.* **263** 114870 (2021)
[23] S Jaballah, H Dahman, I Ghiloufi, G Neri and L El Mir *Int J. Hydrogen Energy.* **45** 34268 (2020)
[24] Q Gao, Y Dai, B Han, W Zhu and X Li *Appl. Surf. Sci.* **490** 178 (2019)
[25] T A Johny, V Kumar and H I ImaiKanno *Thin Solid Films* **520** 5797 (2012)
[26] R Nisha *PhD Thesis* (Cochin University of Science and Technology, India) (2013)
[27] H S Alanazi, N Ahmad and F A Alharthi *RSC advances.* **11(17)** 10194 (2021)
[28] N Aggarwal *J. Mater. Sci. Mater. Electron.* **27** 13006 (2016)
[29] M Kaur, M Shaheera, A Pathak, S C Gadkari and K Debnath *Sensors Actuators B. Chem.* **335** 129678 (2021)
[30] J Agrawal, T Dixit, I A Palani, M S R Rao and V Singh *J. Phys. D Appl Phys.* **51** 18 185106 (2018)
[31] V L Patil, S A Vanalakar, N L Tarwal, A P Patil, T D Dongale, J H Kim and P S Patil *Sensors Actuators A. Phys.* **299** 111611 (2019)
[32] K Punia, G Lal, S Narain and S Kumar *Ceram Int.* **46** 12296 (2020)

[33] X Ren, Z Xu, D Liu, Y Li, Z Zhang, and Z Tang *Sensors Actuators B. Chem.* **357** (2022)
[34] S Sa-nguanprang, A Phuruangrat, T Thongtem and S Thongtem *Russ J. Inorg. Chem.* **64** 1600 (2019)
[35] L Sun, C Hou, J Sun, Q Mo and J Han *Chem.* **367** 131987 (2022)
[36] R S Ganesh et al. *Sensors Actuators A Phys.* **269** 331 (2018)
[37] Y H Zhang, Y L Li, F L Gong, K F Xie, M Liu, H L Zhang and S M Fang *Sensors Actuators, B Chem.* **305** 127489 (2020)
[38] K Diao, J Xiao, Z Zheng and X Cui *Appl. Surf. Sci.* **459** 630 (2018)
[39] S Saini, A Kumar and S Ranwa *Appl. Phys. A* **128** 1 (2022)
[40] T V A Kusumam, V S Siril, K N Madhusoodanan, M Prashantkumar, Y T Ravikiran, and N K Renuka *Sensors Actuators A. Phys.* **112389** (2020)